journal

J. Am. Ceram. Soc., 85 [11] 2799–804 (2002)

Determining Crystal Habits from Observations of Planar Sections

David M. Saylor*

National Institute of Standards and Technology (NIST), Gaithersburg, Maryland 20899

Gregory S. Rohrer*,†

Department of Materials Science and Engineering, Carnegie Mellon University, Pittsburgh, Pennsylvania 15213

A method is described for reconstructing the habits of crystals embedded in a second phase from observations of random planar sections of known orientation. We have generated simulated observations based on five assumed crystal habits and found that it is possible to reconstruct the shape from 100-1000 planar sections, depending on the relative area of each facet. Habit planes comprising as little as 3% of the crystal's area have been detected and axial ratios accurately determined.

I. Introduction

When three-dimensional crystals are embedded in an opaque second phase, they are typically observed only in two-dimensional planar sections. To make true three-dimensional images of such crystals, one must resort either to tomography,[1] which uses microscopic probes that penetrate the sample, or serial sectioning.[2] The former technique requires instrumentation that is not widely available, whereas the latter is labor intensive and limited in resolution. The purpose of this paper is to demonstrate that average three-dimensional crystal habits can be determined by combining the geometric information found in conventional micrographs with crystal orientation data, which can be routinely determined from electron backscattered diffraction patterns in a scanning electron microscope.[3] The method proposed is an adaptation of a procedure originally described by Adams[4,5] to determine the distribution of grain-boundary plane orientations.

We consider here isolated crystalline inclusions dispersed in a second phase. Although we assume that the crystals have a consistent habit, they may vary in size. The required experimental observations include numerous randomly distributed planar sections of the crystals and the orientation of each crystal with respect to the plane of observation. In practice, these observations might be obtained from a single section through a collection of randomly oriented crystals or multiple randomly oriented sections through a collection of crystals with some degree of texture. This problem is relevant to the study of inclusions in two-phase microstructures and composites. Therefore, we imagine a single two-dimensional section through a composite microstructure that intersects many isolated and randomly oriented crystals embedded in a second phase.

We begin by noting that the line segments bounding an observed section of a crystal are formed by the intersection of the crystal's habit planes with the plane of observation. With knowledge of the crystal's orientation, the line segment can be transformed to the crystal reference frame. Although we don't know the actual plane that created the observed line segment, we do know that it belongs to the set of planes whose normals are perpendicular to the segment. On a stereographic projection, these planes lie on a great circle perpendicular to the line segment. If we observe many segments from different crystals, we have a corresponding number of sets of possible planes (each on a different great circle) that might be responsible for the observations. The key to our analysis is that correct habit planes are sampled with a high probability; there is at least one habit plane in each set of possible planes. Therefore, the great circles arising from each observed line segment must intersect at the positions of habit planes. The nonhabit planes, on the other hand, are far more numerous, and therefore each nonhabit plane is observed less frequently than a true habit plane. This basic idea allows a finite set of habit planes to be identified. With this information, each observed line segment can then be assigned a habit plane of origin, and, based on the total length of the segments associated with each facet, the relative areas of the habit planes can be estimated and the average shape defined.

II. Method

For simplicity, we assume that the crystals are fully faceted or that they can be reasonably approximated as such. In this case, all the observed two-dimensional sections of the crystals will be polygons, as illustrated in Fig. 1(a). Consider the *j*th line segment bounding the *i*th crystal section ($\bar{l}_{ij}$). Although we do not know the exact plane that leaves the trace on the plane of observation, we do have two pieces of information that, after the observation of many sections, allow us to deduce the most likely habit plane. First, we know that the habit plane must belong to the set of planes that include the surface trace and obey the condition $\bar{l}_{ij} \cdot \hat{\boldsymbol{n}}_{ijk} = 0$, where the vectors $\hat{\boldsymbol{n}}_{ijk}$ are unit normals to the planes. In other words, the habit plane must be in the zone of $\bar{l}_{ij}$. Second, we know that each plane in the set $\hat{\boldsymbol{n}}_{ijk}$ will not be observed with the same probability. The plane of observation intersects perpendicular planes with the highest probability, and those inclined to the plane of observation with a smaller probability. Taking θ_k to be the angle between $\hat{\boldsymbol{z}}$ and $\hat{\boldsymbol{n}}_{ijk}$ (see Fig. 1(b)), the relative probability of intercepting a plane whose normal is inclined by θ_k from the surface normal is $\sin\theta_k$. We use this information in the following way: for every line segment observed, we have a set of possible planes, $\hat{\boldsymbol{n}}_{ijk}$, that contains a correct habit plane together with a set of incorrect planes. In other words, the probability of a true habit plane orientation being found in each set $\hat{\boldsymbol{n}}_{ijk}$ is 1, whereas the probability of any given nonhabit plane being found in the same set is <1. So, after many sets of planes $\hat{\boldsymbol{n}}_{ijk}$ are observed and transformed into the crystal reference frame (weighted by the observed line length, $|l_{ij}|$, and the probability of observation, $\sin\theta_k$), the frequency with which the true habit planes are observed will greatly exceed the frequency with which nonhabit planes are observed. After identifying a finite list of habit planes, it is then possible to reclassify the observations by habit plane of origin. The ratios of the total line lengths crossing each facet then provide an estimate of the relative areas of the habit planes.[6]

J. E. Blendell—contributing editor

Manuscript No. 187119. Received February 27, 2002; approved August 6, 2002.
This work was supported primarily by the MRSEC program of the National Science Foundation (under Award Number DMR-0079996) and by partially by NASA (under Grant No. 8-1674).

*Member, American Ceramic Society.
†Author to whom correspondence should be addressed.

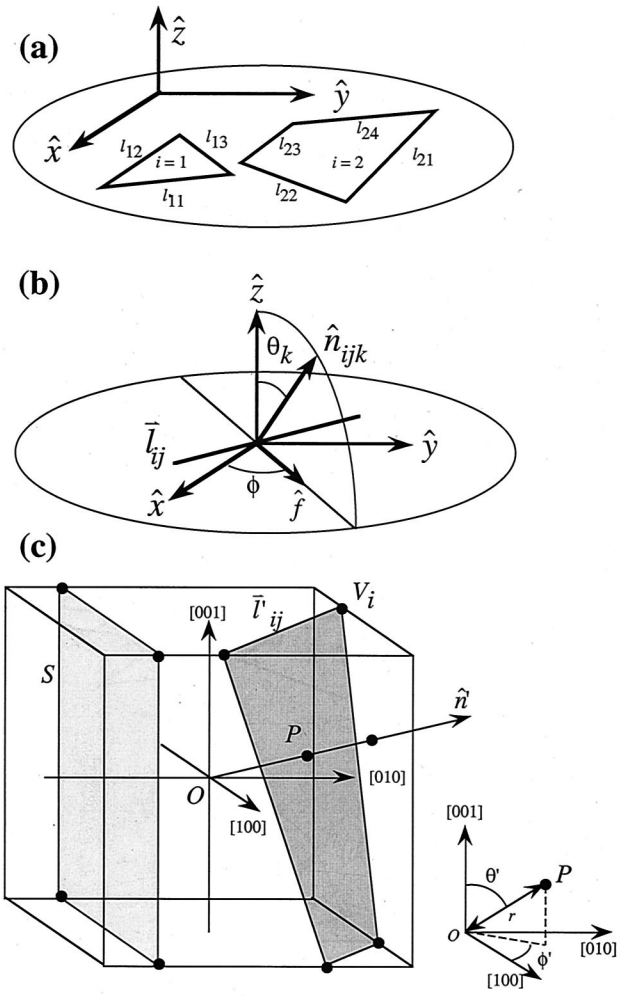

Fig. 1. (a) Observation of the sample in the laboratory reference frame. Polygons are random planar sections of crystals of known orientation. (b) Definition of the variables in the laboratory reference frame. The normal vectors to the possible bounding planes, $\hat{n}_{ijk}$, trace out a circular arc. (c) Two possible random planes are illustrated and quantities in the crystal reference frame are defined.

This procedure is implemented using a set of discrete orientations in the sample and crystal reference frame. In the laboratory frame, every observed line segment, $\bar{l}_{ij}$, can be described by the angle ϕ, which is the in-plane angle between the ***x***-axis and the normal to the line segment ($\bar{f}$), as illustrated in Fig. 1(b). The unit normal vector, $\hat{\boldsymbol{n}}_{ijk}$, to every plane in the zone of $\bar{l}_{ij}$, is described by two angles, ϕ and θ_k, where ϕ is the same for all planes in the set. The domain of the spherical angles ϕ and θ_k is discretized in units of ϕ and cos θ. This partitioning scheme creates discrete units of equal area on the surface of a sphere. The in-plane angle, ϕ, ranges from 0 to π and the out of plane parameter (cos θ_k) ranges from -1 to 1. For the first line segment of each polygon, we find the discrete value of ϕ and add the quantity $|\bar{l}_{ij}|$ sin θ_k to each partition (ϕ, cos θ_k) that corresponds to a plane in the zone of the line segment. The process is repeated for each line segment of the polygon.

Because all the line segments in a polygon belong to the same crystal, the sets of planes can be transformed to the crystal reference frame using the 3×3 matrix, $\mathbf{g}(\phi_1,\Phi,\phi_2)$, where ϕ_1,Φ, and ϕ_2 are the Euler angles and $\mathbf{g}$ is given as[7]

$$\mathbf{g}(\phi_1, \Phi, \phi_2) = \begin{bmatrix} c\phi_1 c\phi_2 - s\phi_1 s\phi_2 c\Phi & s\phi_1 c\phi_2 + c\phi_1 s\phi_2 c\Phi & s\phi_2 s\Phi \\ -c\phi_1 s\phi_2 - s\phi_1 c\phi_2 c\Phi & -s\phi_1 s\phi_2 + c\phi_1 c\phi_2 c\Phi & c\phi_2 s\Phi \\ s\phi_1 s\Phi & -c\phi_1 s\Phi & c\Phi \end{bmatrix} \quad (1)$$

In Eq. (1), c and s represent cosine and sin, respectively. So, the vectors $\hat{\boldsymbol{n}}_{ijk}$ can be transformed to the crystal reference frame, $\hat{n}'$, by

$$\hat{n}'^{l} = \mathbf{g}^{lm}(\phi_1, \Phi, \phi_2)\hat{n}^m_{ijk} \quad (2)$$

where $\hat{n}'^{l}$ are the components of the unit vector in the crystal reference frame and $\hat{n}^m_{ijk}$ are the components of the vector in the laboratory reference frame. Note that throughout the paper, quantities in the crystal reference frame are primed.

The domain of planes in the crystal reference frame is discretized in the same way as the laboratory reference frame. The quantity in each partition (ϕ, cos θ_k) is added to an equivalent partition (ϕ', cos θ') in the crystal reference frame, and all its symmetric equivalents. The process is then repeated using the line segments from all the other observed crystals. With all the sets of planes derived from each observed line segment transformed to the crystal reference frame, we can now define the quantity $\bar{p}(\hat{n}')$ as

$$\bar{p}(\hat{n}') = \frac{\sum_{i,j,k} g_i \hat{n}_{ijk} |l_{ij}| \sin \theta_k}{\sum_{i,j,k} |l_{ij}| \sin \theta_k} \quad (3)$$

The function $\bar{p}(\hat{n}')$ is the probability that a given length of line on the perimeter of a random section plane falls on a plane with the orientation $\hat{n}'$. The normalization factor in the denominator is used so that when $\bar{p}(\hat{n}')$ is multiplied by the number of partitions, the results are produced in multiples of a random distribution (MRD). When this probability is plotted as a function of $\hat{n}'$, maxima will occur at the habit planes.

The maxima in $\bar{p}(\hat{n}')$ allow the selection of a finite list of habit planes that form a convex shape. To specify the exact shape, we need to know the relative areas of each facet. To do this, we calculate the total length of line that intersects each habit plane in the following way. For each observed line segment in the crystal reference, we compute a scalar product with the normal vector of each possible habit plane. As long as the list of habit planes is small, the scalar product will vanish for only one habit plane, and this will unambiguously identify the plane that produced that segment. This condition allows us to assign each line length to one of the particular habit planes. In practice, the origin of those line segments simultaneously perpendicular to more than one habit plane will be ambiguous. Although several ways to assign these lengths to the most probable plane can be imagined, we will simply ignore these segments for now. After all the data has been reclassified in this way, we have the total length of line per habit plane. Because it is known that the total length of a set of randomly distributed lines intersecting an area is proportional to that area, the ratios of the line lengths associated with each habit plane is an estimate of the relative surface areas.[6]

An alternative method for determining the exact shape is to search either the accumulated data or the specimen itself for planar sections that lie perpendicular to more than one distinguishable habit plane. Specifically, one must search for section planes whose normals are parallel to the cross product of two distinguishable habit plane normals (this means the bounding planes are perpendicular to the plane of observation). We shall refer to such observation planes as special sections. Next, the special sections can be sorted to find those that contain two parallel segments from each of the habit planes. For example, consider the special section plane labeled "S" in Fig. 1(c). In this case, the two distinguishable habit planes are {100} and {001}, and the observed polygon consists of line segments in (100), (001), and their parallel complements, $(\bar{1}00)$ and $(00\bar{1})$. The ratio of the perpendicular distances between complementary facets of the same type directly gives the crystal's axial ratio. Assuming multiple special sections of the same type can be located, the results can be averaged and the error estimated. By repeating this process for all pairs of facets on the habit, it is possible to determine the shape.

III. Generating Trial Data Sets

To generate simulated data, one must begin by defining the coordinates of the vertices of the assumed shape. One easy way to

accomplish this is to define the shapes in Wulffman[8] and export the shape as a Geomview[9] geometry file. These files include a listing of all the vertices of the polyhedron, which are also the endpoints of the line segments defining the edges of the crystal. We take random planar sections of this shape in the following way: first, the vertex most distant from the center of the crystal is used to define the radius (R) of an imaginary sphere that encloses the crystal. We then select a random direction ($\hat{n}'$) and point P along this direction that falls within the sphere. This is accomplished by choosing a set of random orientation parameters, based on the Euler angles, ϕ_1, Φ, ϕ_2. To ensure that all possible orientations are selected with equal probability in this inhomogeneous orientation space, values of ϕ_1 and ϕ_2 are selected in the range of 0–2π and a value of $\cos\Phi$ is selected in a range of -1 to 1. The Euler angles are then used to transform the surface normal in a laboratory frame, [001], to a normal for a hypothetical section plane using the following expressions derived from Eq. (2):

$$n_1' = \sin\phi_2 \sin\Phi \tag{4a}$$

$$n_2' = \cos\phi_2 \sin\Phi \tag{4b}$$

$$n_3' = \cos\Phi \tag{4c}$$

In Eq. (4), n_i' are the components of $\hat{n}'$ along the crystal axes. To convert from Euler angles to the spherical angles in the crystal reference frame, we note that $\theta' = \Phi$ and $\phi' = \pi/2 - \phi_2$. The distance, r, from the center of the crystal to the point P, is then randomly selected such that $0 \leq r \leq R$. These quantities, as defined in Fig. 1(c), allow us to define a plane perpendicular to $\hat{n}'$ at the point P. Every line segment that forms an edge of the polyhedron is then tested for an intersection with the randomly selected plane. When the plane intersects two segments bounding the same habit plane, the points of intersection (V_i) define an observed line segment on the plane of observation.

When all the line segments defining a given polygon in a random plane are identified, they are transformed back to the sample reference frame in the following way:

$$\vec{l}_{ij} = \mathbf{g}^T \vec{l}_{ij}' \tag{5}$$

In Eq. (5), $\mathbf{g}^T$ is the transpose of the matrix in Eq. (1) (in this case, $\mathbf{g}^{-1} = \mathbf{g}^T$). A unit normal is determined for each line segment, and the angle ϕ is determined as the angle between each segment's normal and the x-axis. Now, we have a set of Euler angles and the lengths and directions of line segments that make up a random section plane. The process is repeated to accumulate the trial data set, which can be analyzed according to the description in Section II.

IV. Results

To test the method, we have generated test data for five crystal habits. For all results presented here, we have partitioned each of the orientation parameters into 60 parts. Therefore, the resolution is ~3°. We first consider a crystal with cubic symmetry, bounded by {100} and {111} planes, as depicted schematically in Fig. 2(a). Using this assumed shape, the function $\bar{p}(\hat{n}')$ was calculated based on 50, 100, 10^3, and 10^4 trial observations. The result for 100 planar sections is illustrated in Fig. 2(b), plotted in stereographic projection along the [001] axis. We have found that it is easier to visualize the results by examining oblique projections of three-dimensional renderings of $\bar{p}(\hat{n}')$, as illustrated in Fig. 3. In this case, the heights of the features in the plots are proportional to the value of $\bar{p}(\hat{n}')$; the in-plane coordinates are identical to those used in the stereographic projection in Fig. 2(b). In all four cases, the {100} and {111} habit planes are easily identified by the local maxima at these positions. Therefore, the habit for this particular form could be determined from as few as 50 random observations. The results were not significantly different in trials using a coarser partitioning scheme (6°).

In Fig. 3, the peaks at the {100} positions are much larger than those at the {111} positions because the {100} planes make up a greater portion of the surface area on this particular shape. However, it should be noted that the relative values of the maxima in $\bar{p}(\hat{n}')$ are not reliable quantitative indicators of the relative surface area. For example, in this case, the ratio of the maximum at {100} compared with that at {111} is ~3.5. When one accounts for the multiplicity difference, this would imply that the probability of observing a line segment from a {100} plane is 2.62 times that of observing a {111} plane. In fact, the surface area ratio is 8.72. One reason that the intensities are not correlated directly to the areas is that there is a variable background of erroneously assigned line segments. Partitions corresponding to true habit planes will contain correct assignments along with several incorrect assignments. Partitions corresponding to nonhabit planes will contain a variable number of incorrect assignments; the exact number depends on the distribution of habit planes and the proximity of a given partition to a habit plane. Other sources of error in the function $\bar{p}(\hat{n}')$ are described in Section V.

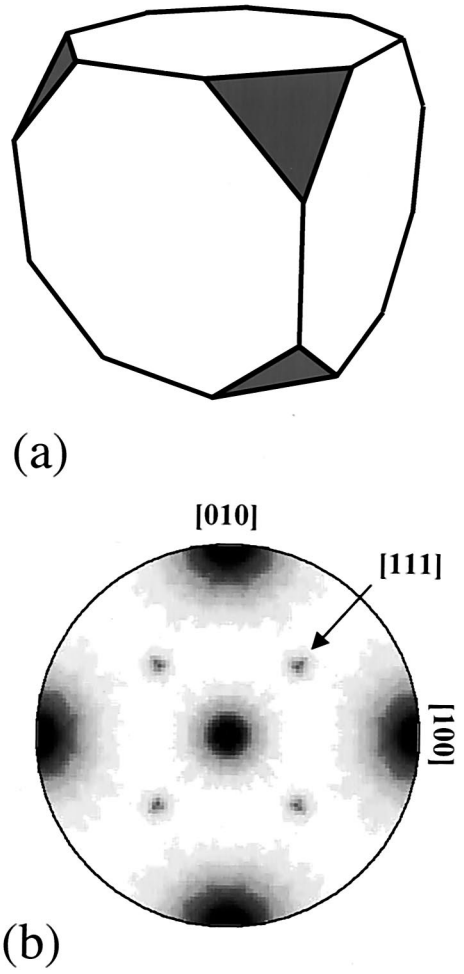

Fig. 2. (a) Schematic of the assumed habit ("c1"). Small triangular faces are {111}. (b) Plot of the function $\bar{p}(\hat{n}')$, in stereographic projection along the [001] for the shape depicted in Fig. 2(a). In the plot, the darkness of the shading corresponds to the magnitude of $\bar{p}(\hat{n}')$. MRD values are in the range of 0.5–6.6.

To determine the surface area ratio from our observations, we must reclassify the observations and assign each of the line segments to one of the two habit planes. The estimated area ratios are given in Table I. Note that all estimated area ratios for this shape (referenced as "c1") are within 8% of the actual value. Because this is based on the total area, the error in the area of any particular facet is actually much smaller. This is illustrated by examining the axial ratio, which we define as the ratio of the perpendicular distances from the center of the crystal to two distinguishable facets (l_{100}/l_{111}). For the shape in question, an 8% error in the ratio of areas leads to an error in the axial ratio of

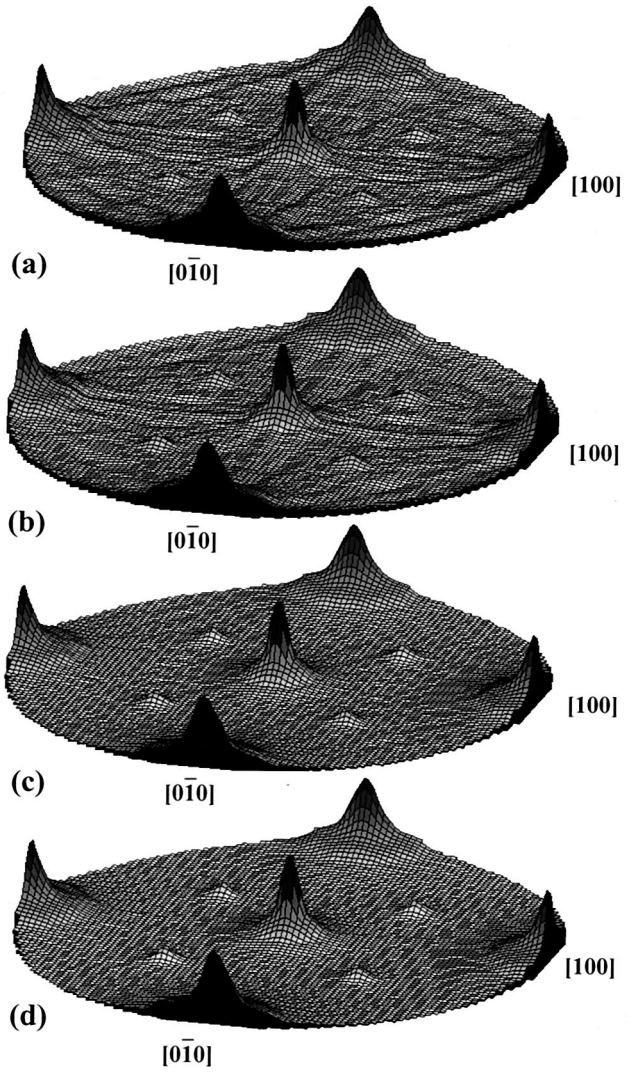

Fig. 3. Three-dimensional renderings of $\bar{p}(\hat{n}')$ for the shape depicted in Fig. 2(a). The function was calculated based on (a) 50 (MRD range of 0.5–7.0), (b) 100 (MRD range of 0.5–6.6), (c) 10^3 (MRD range of 0.7–6.6), and (d) 10^4 planar sections (MRD range of 0.7–6.6).

<1%. For the purposes of reconstructing a crystal shape, we consider this level of error to be acceptable.

Tests on other shapes gave similar results, which are summarized in Fig. 4 and Table I. As expected, we find that as the number of distinct facets increases, or area ratios increase, more observations are required to accurately determine relative areas. For example, the two anisotropic shapes with orthorhombic symmetry in Figs. 4(c) and (d) have one set of facets that are approximately one-tenth and one-twentieth the area of the largest facet. For the most anisotropic shape, referenced as "o2," in which the {010} surfaces comprise <3% of the entire surface area, the small peaks at the {010} positions are apparent only when plotted on a logarithmic scale. Furthermore, the value of $\bar{p}(\hat{n}')$ at (010) is not significantly larger than the amplitude of the background falling on the great circles connecting the {100} positions. Finally, whereas the shapes of the more isotropic crystals are determined from only 100 observations, 1000 observed section planes were required to accurately determine the shape of the more anisotropic crystals.

To quantify the errors involved in this process, the relative areas were determined in five separate trials with different sets of randomly generated data. The results from the five trials were used to calculate an average area ratio and a standard deviation. The results are summarized in Table II. As expected, the standard deviation is smaller as the number of observations increases. Furthermore, the standard deviation increases with the anisotropy of the shape.

V. Discussion

The results presented in Section IV verify that the method described in this paper can be used to reconstruct the habits of faceted crystals from random sections. Furthermore, the number of observations required seems feasible from an experimental point of view. In most cases, the observation of only 100 planar sections should be sufficient. For very anisotropic shapes, as many as 1000 observations might be required. However, this number is well within the capability of conventional orientation imaging microscopy.

Beyond experimental errors in the measurement of angles and lengths, there are a number of errors inherent in the method that we have described. It has already been mentioned that the relative values of the local maxima of $\bar{p}(\hat{n}')$ are not reliable indicators of relative areas. This is primarily because the erroneously assigned line segments are not distributed homogeneously. The probability of an erroneous assignment in any given partition is a function of the angular separation from a true habit plane. Although it is possible to quantify this error and subtract a background from $\bar{p}(\hat{n}')$, we leave this calculation for a future paper and note that the current solution provides reasonably accurate results.

The discretization of the domain of orientations also creates errors in the function $\bar{p}(\hat{n}')$. Each observed line segment corresponds to sets of planes whose normals define a great circle on the stereographic projection. However, because we have discretized ϕ, the great circle of possible habit planes will be rotated from its true position to the center of the partition. Furthermore, the contribution from each line segment is added to every partition that the great circle crosses, even though the centers of these partitions will not necessarily lie on the great circle. Both of these factors cause the maxima of $\bar{p}(\hat{n}')$ to increase in breadth. In practice, it is possible to refine the discretization so that the resulting errors are much smaller than the experimental uncertainty.

Additional errors arise because we reduce the zone of possible habit planes to a finite set of plane normals at discrete intervals. Because the space of spherical angles is inhomogeneous, there is not necessarily a one-to-one association between the partitions in a zone in the laboratory reference frame and partitions in a zone in the crystal frame. Therefore, contributions from distinct planes in

Table I. Geometric Data for Actual and Estimated Shapes

	Axial ratio	Actual area ratio	Estimated area ratio			
			50 obs.	10^2 obs.	10^3 obs.	10^4 obs.
c1	$l_{100}/l_{111} = 0.71$	$A_{100}/A_{111} = 8.72$	9.21	7.98	9.15	9.01
c2	$l_{100}/l_{111} = 0.86$	$A_{100}/A_{111} = 1.8$		1.75	1.89	
c3	$l_{110}/l_{100} = 1$	$A_{110}/A_{100} = 1.58$		1.57	1.60	
	$l_{111}/l_{100} = 1$	$A_{111}/A_{100} = 1$		0.97	0.91	
o1	$l_{100}/l_{010} = 0.105$	$A_{100}/A_{010} = 9.5$		12.0	10.0	
	$l_{001}/l_{010} = 0.210$	$A_{001}/A_{010} = 4.75$		6.30	5.10	
o2	$l_{100}/l_{010} = 0.053$	$A_{100}/A_{010} = 19$		26.9	20.4	
	$l_{001}/l_{010} = 0.105$	$A_{001}/A_{010} = 9.5$		13.5	10.3	

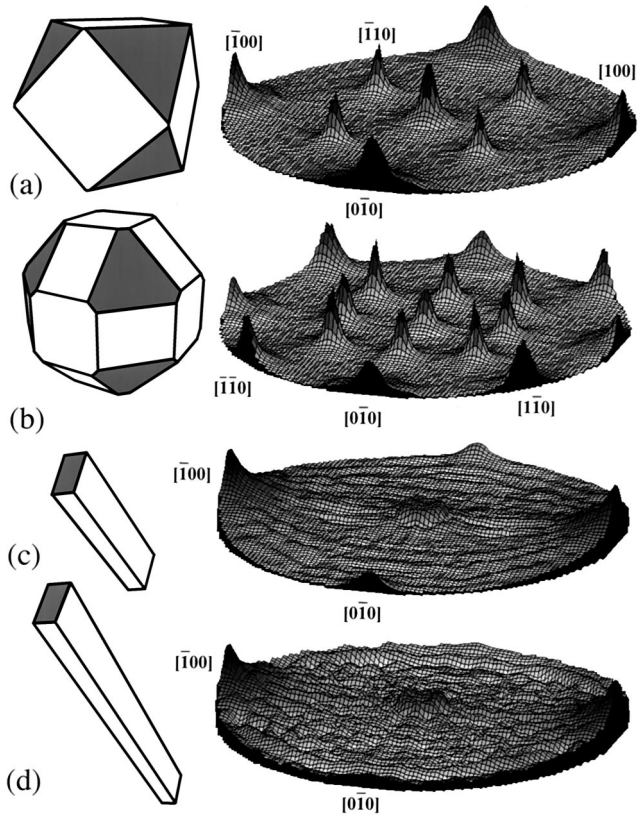

Fig. 4. Three-dimensional renderings of $\bar{p}(\hat{n}')$, for the shapes referenced as (a) "c2," (b) "c3," (c) "o1," and (d) "o2." In each case, the function was calculated based on 10^3 planar sections. Note that a different scale is used to increase the dynamic range in Figs. 4(c) and (d). In Figs. 4(a) and (b), shading is used to indicate {111} facets. In Figs. 4(c) and (d), the shading indicates {010}. MRD ranges for Figs. 4(a) and (b) are 0.8–4.9 and 0.8–3.8, respectively. Ranges of ln (MRD + 1) for Figs. 4(c) and (d) are 0.2–3.0 and 0.3–2.9, respectively.

the laboratory space, when transformed to the crystal space, might be added to a single partition. For the same reason, partitions in the crystal space that actually lie on the great circle of possible plane normals may not receive any contributions from a set of planes observed in the laboratory frame.

Our approach of reclassifying the data and assigning each line segment to a habit plane makes our results insensitive to errors in the relative values of $\bar{p}(\hat{n}')$ that arise from a combination of the factors described above. However, the method we use to assign the origin of the line segments will also introduce some error. Because we are ignoring line segments of questionable origin, we are not sampling all configurations with equal probability. There are several ways one might assign the ambiguous planes and reduce the associated error. For example, the ambiguous lines could be assigned to the habit plane most nearly perpendicular to the sample surface. A two-step process is also possible, in which the ambiguous line segments are first excluded, and later assigned to habit planes with a probability reflecting area fractions that result from the initial calculation. Although these procedures seem unnecessary now, they might be required for habits that contain a greater number of distinct facets.

We initially assumed that the crystals were completely faceted. In practice, the habit might contain a combination of flat and curved segments. The method described here can still be used to determine the relative area of the facets and the axial ratios. However, to determine the exact shape, it will be necessary to know which orientations make up the continuously curved regions and the distance from the center to each point along the curve. It should be possible to obtain this information from the observation of special section planes perpendicular to two distinguishable facets, as described in Section II. An alternate solution is to correct $\bar{p}(\hat{n}')$ by subtracting the inhomogeneous background of erroneous assignments so that it is quantitatively related to the relative area.

We have not yet considered how a dispersion of shapes would affect the results. For example, we might expect a set of crystals not in their equilibrium shape to display the same habit planes but to have different axial ratios. In this case, the method described could still be used to identify the habit planes, but the relative areas would represent an average of the sampled crystals.

There are several potentially useful applications for this method. One obvious application is to determine equilibrium crystal shapes and, by application of the Wulff construction, the relative surface energies. In a single-phase material, this can be accomplished by using cavities or voids within a crystal, sometimes referred to as negative crystals.[10,11] In a typical sintered material, small pores will be trapped within grains as boundaries migrate past them. If annealed long enough, these pores will reach an equilibrium shape. A polished plane through the bulk of such a ceramic will reveal random sections of grains with different orientations and, therefore, random sections of pores. The method might also be used to determine relative interface energies in two-phase materials. For example, consider annealing small crystals in a high-volume fraction of a liquid phase (where coarsening is suppressed by long diffusion lengths). Observations of a random section plane through the quenched solid can then be used to determine the crystal's equilibrium shape in the liquid. The method described here might also be useful to determine average particle shapes and aspect ratios in two-phase materials and composites, even when the crystals are not strictly self-similar. Knowledge of an average shape will make it possible to develop reliable three-dimensional models as input for computer-based simulations.

VI. Summary

Observations of random planar sections of crystals can be used to determine the habit and axial ratios. Our simulations show that it is possible to reconstruct shapes containing three distinguishable facets based on 100-1000 observations, depending on the anisotropy of the crystal form. The method should be useful for determining equilibrium shapes and relative interfacial energies.

References

[1]H. F. Poulsen, S. F. Nielsen, E. M. Lauridsen, S. Schmidt, R. M. Suter, U. Lienert, L. Margulies, T. Lorentzen, and D. Juul Jensen, "Three-Dimensional Maps of Grain

Table II. Size of Errors Associated with the Shape Determination

		Average estimated area ratio/standard deviation (5 trials)			
	Actual area ratio	50 obs.	10^2 obs.	10^3 obs.	10^4 obs.
c1	$A_{100}/A_{111} = 8.72$	8.79/1.26	8.70/1.09	9.08/0.15	9.00/0.05
c2	$A_{100}/A_{111} = 1.8$		1.81/0.09	1.88/0.04	
c3	$A_{110}/A_{100} = 1.58$		1.63/0.10	1.58/0.05	
	$A_{111}/A_{100} = 1$		0.94/0.07	0.90/0.03	
o1	$A_{100}/A_{010} = 9.5$		9.74/3.28	9.41/0.43	
	$A_{001}/A_{010} = 4.75$		5.02/1.28	4.70/0.33	
o2	$A_{100}/A_{010} = 19$		22.26/6.73	19.02/1.26	
	$A_{001}/A_{010} = 9.5$		11.18/2.47	9.41/0.60	

Boundaries and the Stress State of Individual Grains in Polycrystals and Powders," *J. Appl. Crystallogr.*, **34** [6] 751–56 (2001).

[2]J. Alkemper and P. W. Voorhees, "Three-Dimensional Characterization of Dendritic Microstructures," *Acta Mater.*, **49** [5] 897–902 (2000).

[3]B. L. Adams, S. I. Wright, and K. Kunze, "Orientation Imaging: The Emergence of a New Microscopy," *Metall. Trans. A*, **24** [4] 819–31 (1993).

[4]B. L. Adams, "Description of the Intercrystalline Structure Distribution in Polycrystalline Materials," *Metall. Trans. A*, **17** [12] 2199–207 (1986).

[5]R. J. Larsen and B. L. Adams, "New Stereology for Recovering Grain Boundary Character Distributions in the Crystal Frame"; pp. 27–29 in *Proceedings of Plasticity '02*. Edited by A.S. Khan and O. Lopez-Pamies. Neat Press, Fulton, MD, 2002.

[6]M. G. Kendall and P. A. P. Moran, *Geometrical Probability*; pp. 78–80. Hafner Publishing Co., New York, 1963.

[7]H.-J. Bunge, *Texture Analysis in Materials Science*; p. 21. Translated by P.R. Morris. Butterworths, London, U.K., 1982.

[8]Wulffman, public domain software available from the Center for Theoretical and Computational Materials Science at the National Institute for Standards and Technology (www.ctcms.nist.gov).

[9]Geomview, public domain software available from the Geometry Center, Minneapolis, MN (www.geom.umn.edu/).

[10]J.-H. Choi, D.-Y. Kim, B. J. Hockey, S. M. Wiederhorn, C. A. Handwerker, J. E. Blendell, W. C. Carter, and A. R. Roosen, "Equilibrium Shape of Internal Cavities in Sapphire," *J. Am. Ceram. Soc.*, **80** [1] 62–68 (1997).

[11]M. Kitayama, T. Narushima, and A. M. Glaeser, "The Wulff Shape of Alumina: II, Experimental Measurements of Pore Shape Evolution Rates," *J. Am. Ceram. Soc.*, **83** [10] 2572–82 (2000). □